An Unsupervised Group Average Cortical Parcellation Using Diffusion MRI to Probe Cytoarchitecture

Tara Ganepola, Zoltan Nagy, Daniel C. Alexander, and Martin I. Sereno

Abstract Cortical parcellations provide valuable localisation resources for other neuroimaging modalities such as fMRI as well as insight into the structure-function relationship of the brain. The venerable but now dated ex vivo Brodmann map is currently being superseded by in vivo techniques that can better take into account intersubject variability. One popular in vivo method focusses on myeloarchitecture by measuring T1. This, however, probes only one aspect of cortical microstructure and is less useful in regions of low myelination. In contrast, diffusion MRI (dMRI) is sensitive to several additional microstructural features and can potentially provide a richer set of information regarding the architecture of grey matter microcircuitry. The following study used 3T HARDI data of multiple subjects to produce an entirely unsupervised, hemisphere-wide, group-average, parcellation. A qualitative assessment of the resulting cortical parcellation demonstrates several spatially coherent clusters in areas corresponding to well known functional anatomical areas. In addition, it exhibits some cluster boundaries that correlate with independently derived myelin mapping data for the same set of subjects, whilst also providing distinct clusters in areas (e.g., within MT+) where myelination is a less informative measurement.

T. Ganepola (✉)
Department of Cognitive, Perceptual and Brain Sciences, University College London, London, UK

Department of Computer Science, Centre for Medical Image Computing, University College London, London, UK
e-mail: tganepola@gmail.com

Z. Nagy
Laboratory for Social and Neural Systems ResearchUniversity of Zurich, Zurich, Switzerland

Wellcome Trust Centre for Neuroimaging, UCL Institute of Neurology, London, UK

D.C. Alexander
Department of Computer Science, Centre for Medical Image Computing, University College London, London, UK

M.I. Sereno
Department of Cognitive, Perceptual and Brain Sciences, University College London, London, UK

A. Fuster et al. (eds.), *Computational Diffusion MRI*, Mathematics and Visualization, DOI 10.1007/978-3-319-54130-3_12

1 Introduction

The cytoarchitecture of the cerebral cortex in humans and many other mammalian species was first investigated in the early 1900s using histological sections of post-mortem brains stained for cell bodies or myelinated fibers. Pioneers of this era [1–3] discovered that the microstructure of the cortex was organised into six layers, the columnar appearance of which varies throughout the cortical sheet. Roughly homogeneous modules of variable size were observed and attributed to functional specificity, starting with striate cortex whose border with V2 is easily visible to the naked eye in hand-cut unfixed tissue. The hypothesis of a mosaic of internally homogeneous areas prevails today and these classical parcellations have been widely adopted in modern studies, for example, to localise activation foci in functional imaging studies.

Despite their pervasiveness, it is evident that traditional cortical maps suffer many methodological limitations. One limitation is observer dependant bias, [4]. Another problem is that histological methods are often restricted to a single cell stain per specimen, thus requiring the observer to combine identified boundaries across differently distorted adjacent sections. These limitations may explain the variability in size, location and number of cortical areas reported by different such methods [4–7]. The labour-intensive process of histological sectioning enforces further limits on the sample size used to generate such cortical maps. Subsequent studies have demonstrated a large degree of intersubject variability with regards to the exact location and extent of several well-defined cortical areas. Given this, classical maps derived from a small sample of cadaver brains, are unlikely to accurately reflect boundary definitions for the entire population. Other considerations include the introduction of artefacts from histological sectioning (e.g., including unique nonlinear distortions in each section due to slide mounting and outright tears in the tissue), which complicate registration of data back into undistorted 3D space.

Despite their lower resolution, in vivo methods have the potential to overcome some of these limitations—in vivo analysis provides observer independent image processing, much larger samples sizes, the possibility of multi-modal studies, and completely avoids histology artefacts. Thus far, in vivo investigations of cortical microstructure have focussed predominantly on myeloarchitectonics, via quantitative T1 [8] and R1 (1/T1) mapping [9–11] mapping using multiple flip angles, the ratio of T1-weighted over T2-weighted images [12, 13], and multiple inversion times (MP2RAGE). However, myelination density provides only a partial picture of cortical microstructure. More recently, Glasser et al. extended their T1-weighted/T2-weighted methods into a multi-modal framework for cortical mapping [14]. This approach combined myelin maps , resting state, and task-based functional MRI measures of approximately 200 subjects with expert anatomical knowledge and a complex processing pipeline to produce a semi-automated, group-average, full-hemisphere, cortical parcellation. Nevertheless, the datasets in that paper do not directly measure the fine-grained structural information that is associated with the cyto- and myeloarchitecture of the cortex. For investigators

wishing to acquire a detailed understanding of the structure-function relationship in the cortex, it may be desirable to include measurements of additional features that characterise grey matter (GM) micro-environments.

There is a growing body of evidence [15–22] to support the use of diffusion MRI in cortical imaging facilitated by recent technological advancements, such as multi-band excitation, magnetic field probes [23], and ultra high field imaging. In particular, investigators have demonstrated changes in the dominant diffusion direction between the primary somatosensory and motor cortices, via a measure of radiality [20]. Others have shown the relationship between cortical gyrencephaly and diffusion tensor metrics [21]. Nagy et al. demonstrated the in vivo individualised discriminative power of a feature set derived from high angular resolution diffusion imaging data by testing distinct fMRI-based regions of interest [22]. These findings suggest that dMRI in grey matter may provide an additional informative modality for replicating and possibly refining/redefining the boundary definitions of existing cortical parcellation approaches.

The dMRI signal is sensitive to several microstructural features, including but not limited to axon diameter, neurite density, and dominant fibre direction and hence may offer additional structural information beyond bulk myelination density alone. To test the idea that grey matter dMRI might provide a richer description of cortical microenvironments, we used unsupervised, surface-normal-based, group-average cortical parcellation derived from dMRI-based measures of cytoarchitecture. We applied and refined the framework initially developed by Nagy et al. [22] to a large group of subjects using surface-based and surface-referenced cross-subject averaging of dMRI to obtain a hemisphere-wide map of grey matter diffusion patterns from high resolution, 3T data. The resultant parcellation exhibits several coherent clusters that correspond closely with the locations of well-known cortical areas, despite the classifier having no prior information or non-local spatial constraints of any kind.

2 Methods

2.1 Data and Pre-Processing

Imaging datasets for 17 unrelated subjects (10m, 7f aged 22–35) were randomly selected from the minimally pre-processed, 500-Subjects release of the Human Connectome Project (HCP). For a thorough description of the protocols and pre-processing pipelines refer to the HCP documentation [24–26]. In brief, data were collected on a Siemens 3T Skyra system. Each diffusion dataset comprised of 270 gradient directions, acquired evenly across three interleaved b-shells, b = 1000, 2000 and 3000 s/mm^2. An additional eighteen b=0 images were interleaved throughout the acquisition. The high angular and spatial (1.25 mm isotropic) resolution of the HCP datasets lends itself to investigations of grey matter diffusion where, partial volume effects and low anisotropy values are limiting factors.

The HCP pre-processing steps conducted prior to data release, include eddy current and motion correction, providing diffusion weighted images with good alignment and without major distortions. Therefore, further corrections to this end were not performed; however, HCP diffusion datasets suffer from subject specific gradient nonlinearities that were corrected for during the fitting procedure of the tissue model below.

2.2 Surface Reconstruction

In order to utilise the high resolution (0.7 mm isotropic) of the available structural data we chose the `HCP FreeSurfer` pipeline over the standard `recon-all` pipeline to generate cortical surface reconstructions for each subject. This improved pipeline does not down-sample the T1w images to 1 mm isotropic resolution, and incorporates the additional information available in the T2w scans to reduce surface placement errors [25].

Following cortical surface reconstruction the diffusion datasets of each subject were sampled at the midpoint between the white/grey matter (WM/GM) boundary and the pial surface so as to reduce the likelihood of either WM or CSF contamination [20, 22].

2.3 Feature Space

In a similar procedure to that of Nagy et al. [22], a sixth order spherical harmonic series (SHS) was fit to the dMRI signal in order to characterise the apparent diffusion coefficient (ADC) profile of the cortical tissue. A SHS was fit separately in each b-shell for each surface vertex of the right hemisphere of each subject. A subset of the features presented in [22] were calculated from the ADC to obtain a [1×5] feature vector per vertex, per b-shell. The features, as detailed below, characterise the ADC profile in relation to the local surface normal, and therefore describe the GM tissue irrespective of the orientation differences that result from cortical folding.

1. The value of the ADC profile along the surface normal.

$$f(\mathbf{n})$$

2. The mean of the ADC profile in the plane perpendicular to the surface normal, i.e. parallel to the cortical sheet. $C(\mathbf{n})$ is the unit circle perpendicular to n.

$$\bar{f}_{\perp} = (2\pi)^{-1} \int_{C(\mathbf{n})} f(x)dx$$

3–5. The k=2,3 and 4 moments, respectively, of the ADC in the plane perpendicular to the surface normal.

$$M_{k,\perp} = \int_{C(\mathbf{n})} [f(x)]^k dx$$

The group average of each of the 15 features was computed in turn using sulcus-based surface averaging [27]. This approach allows an individual's folding pattern to be aligned to an average folding pattern, in this case on the `fsaverage` surface. With this method, any given `fsaverage` vertex will combine data from individual subject vertices that have surface normals in different directions. This makes it possible to detect local-surface-geometry-dependent diffusion signatures of cortical areas even though their local normal directions might differ from subject to subject. This information would be compromised if the diffusion data were to be directly averaged in 3D (folded) space. The transformation between each subject's cortical surface and the target brain space was applied to each of the cortical features in turn. The mean across all subjects of each feature was then calculated for each vertex of the `fsaverage` surface. Finally, the averaged features were recombined into a [1×15] group average feature space for classification.

2.4 Classification

The unsupervised classification algorithm, k-means [28], was implemented to parcellate the group average feature set. Several values of k were tested on a trial and error basis, starting with $k = 40$, approximately the number of Brodmann areas. At lower values, the parcellation produces large smooth clusters, and doesn't provide additional structural information to the myelin density map (see below). Results are shown for a value of $k = 150$. At this value the parcellation displayed many more area-like clusters than for lower values, whereas, increasing beyond this value did not provide additional information in initial qualitative assessments. Furthermore, $k = 150$ was the value after which decreases in the sum of total distances for the clustering solution began to plateau, and the total runtime began to increase rapidly (Fig. 1).

Since the clusters are numbered arbitrarily by the algorithm, we included an additional ordering step whereby clusters were reordered by the similarity of cluster centres, starting with the pairing which had the highest affinity. Here, similarity was defined as the Euclidean distance between the mean feature vector of each cluster. This additional ordering stage acts to smooth to the results when viewed on the surface, compared to a completely randomised cluster order.

The resulting group average cortical parcellation was qualitatively compared to a group average myelin map, estimated from the T1w/T2w ratio of the same set of HCP subjects.

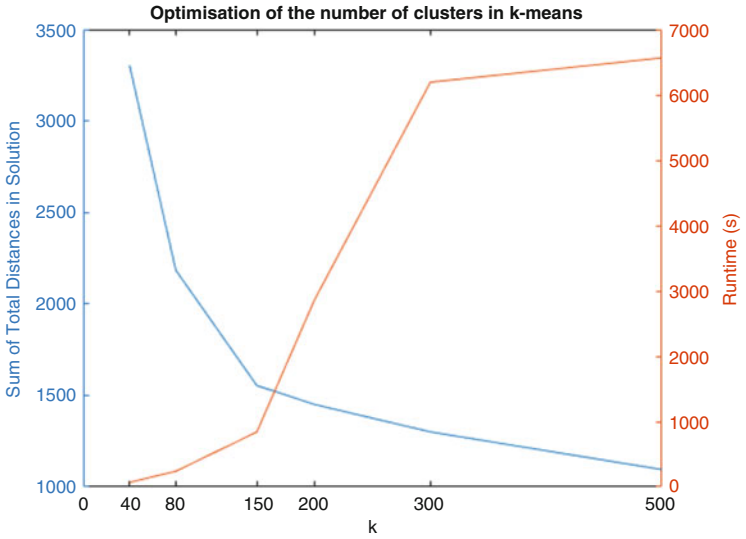

Fig. 1 The tested values of k for the k-means algorithm against the best sum of total distances for each clustering solution (*blue*) and the total runtime of the algorithm in seconds (*orange*)

3 Results

Figure 2 shows the lateral view of the group average diffusion MRI based parcellation (right) alongside the group average myelin map (T1w/T2w) for the same set of subjects (left) on the inflated `fsaverage` surface. Figure 4 shows the medial view of the same. Figure 3 shows the distribution of myelin measurements within regions of interest (ROI) selected from the dMRI parcellation.

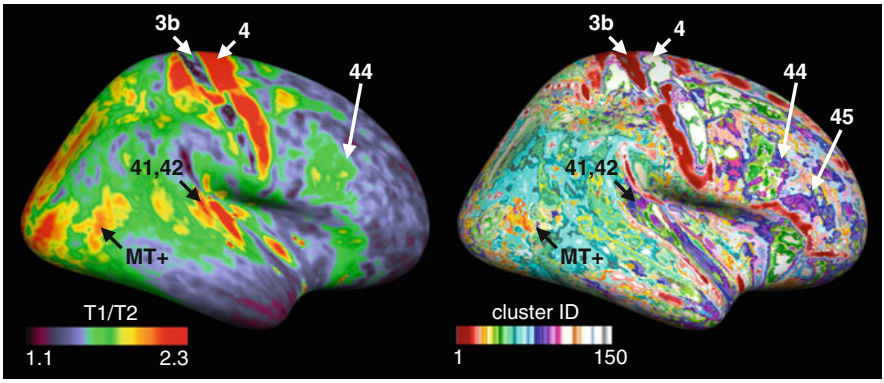

Fig. 2 The lateral view of the diffusion-based parcellation (*right*) and the group average myelin map (*left*)

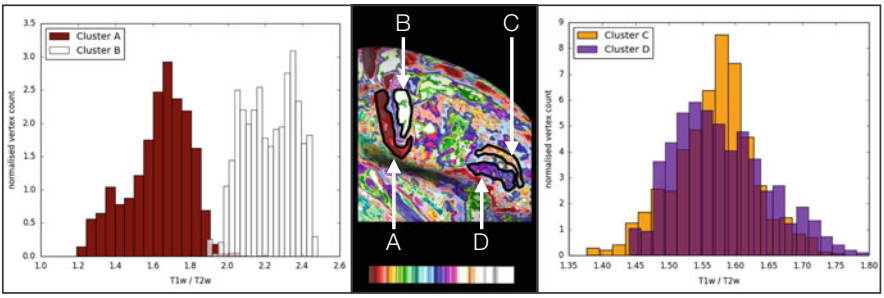

Fig. 3 The distributions of myelin measurements corresponding to regions of interest from the dMRI parcellation result. The histograms on the *left* show T1w/T2w distribution from regions A and B within the central sulcus and are distinct in both modalities. The histograms on the right correspond to regions C and D which appear distinct in the parcellation but have closely overlapping myelin distributions. The outlines of the regions of interest from which the histogram data were extracted are shown in the centre image

3.1 Central Sulcus

The most salient feature of the parcellation is the emergence of distinct and spatially coherent clusters along the anterior (white cluster) and posterior (red cluster) banks of the central sulcus. These have been provisionally labelled 3b and 4 due to their consistency with the location and extent of Brodmann areas 3b and 4. These cortical areas correspond to part of primary somatosensory cortex (S-I) and to primary motor cortex (M-I), respectively. Comparison with the myelin map (left) indicates that the white cluster ID correlates with an area of high myelination, whereas, the red cluster correlates with a drop in myelination. Figure 3 confirms that both the myelin and diffusion measurements discriminate these regions. However, the independently derived diffusion based parcellation produces a more spatially coherent area along the posterior bank of the central sulcus, when compared to the variability of the myelin map in Fig. 2.

There are several factors that may have lead to the group average parcellation exhibiting the closest agreement to the Brodmann map within the central sulcus. The boundary between S-I and M-I represents one of the most prominent transitions within the cortex [20, 29]. The input layers of S-I possess many small cell bodies giving it a granular appearance. In contrast, long cortico-spinal projections in M-I result in large pyramidal cell bodies known (in the foot representation) as Betz Cells, giving an agranular appearance. S-I also exhibits highly myelinated tangential bands of Baillarger, which are less prominent in M-I. Furthermore, in vivo studies at 7T support the hypothesis that differences in the laminar composition between these two regions are manifested in dMRI signal [20].

Another factor which may have improved the detection of these areas is that they demonstrate relatively low intersubject variability. S-I occupies the posterior bank of the central sulcus and extends back into the postcentral gyrus and M-I

occupies anterior bank of the central sulcus, extending forwards into the precentral gyrus, with their transition consistently located at the fundus of the central sulcus [5, 29] near the location of area 3a, which receives predominant input from muscle receptors. This is consistent with the location and extent of the red and white clusters in the parcellation. Therefore, it is likely that architectural changes in these regions, as characterised by their feature vectors, are reinforced by averaging across multiple subjects.

3.2 Broca's Region

Areas 44 and 45 are collectively referred to as Broca's region , which has long been implicated in the production and recognition of speech. We note that both the parcellation and myelin map exhibit a distinct region that is consistent with the location of area 44. This area emerged as a coherent patch despite it not having a consistent relation to macroscopic landmarks in the majority of subjects [6].

In addition, anterior to area 44, we note the presence of a spatially coherent purple/blue cluster, provisionally labelled area 45. It seems that area 45 has no counterpart in the myelin map, supporting the notion that diffusion based cortical imaging may be able to provide additional information to myelin mapping, particularly in areas of lower myelination such as the premotor and prefrontal cortex. This notion is further supported in Fig. 3 where it is clear that the distribution of myelin values between area 45 and the adjacent ROI are very similar. In contrast, these two regions could be differentiated in the diffusion based feature set. The frontal lobe of the diffusion-based parcellation appears more like a patchwork of distinct clusters, whereas the myelin map in this region appears more homogenous.

3.3 Auditory Areas

On the temporal lobe we note that both the myelin map and diffusion-based parcellation exhibited distinct patches that roughly coincide with primary auditory core and belt areas (BA 41 and 42). This suggests that some structural information in the dataset is maintained despite Heschl's gyrus exhibiting a markedly variable folding pattern across subjects [30].

3.4 Occipital Areas

On the right hand side of Fig. 4 the posterior occipital lobe contained prominent purple, blue, and red clusters, giving it a distinct appearance compared to much of the rest of the medial cortical sheet, which was assigned predominantly to green and

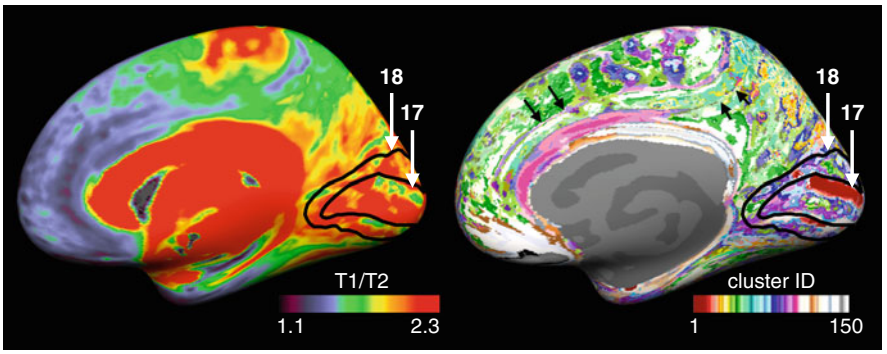

Fig. 4 The medial view of the diffusion-based parcellation (*right*) and the group average myelin map (*left*)

white clusters. This generally correlates with the high myelination of this region, seen in the T1/T2 data at the left of Fig. 4; however it is worth noting that the region of apparent heavy myelination in V2 just below the tip of the "18" arrowhead projected further in the superior direction than the purple region in the diffusion-based result.

The black contours outline the inner and outer extents of area 18 from the FreeSurfer probabilistic atlas, i.e the secondary visual area V2. The inner boundary of this contour corresponds to the neighbouring primary visual cortex, V1 (area 17), within the calcarine sulcus. Despite V1 possessing a prominent tangential band in layer 4B that is lacking in extrastriate area V2 [5, 17], we did not observe distinct coherent clusters corresponding to the full extent of these two areas in either the T1/T2 data or the diffusion data. Instead the most salient feature of this region was the red cluster, which is located near the upper vertical meridian of V1. It is unclear why the boundary of V1 was characterised uniquely by the dMRI feature set, rather than the entire region. However, the myelin map showed a significant decrease in myelination in the same location that is not consistent with the underlying anatomy. This suggests the presence of a systematic surface placement error that my have resulted in CSF partial voluming in both data sets, which resulted in a region near the upper and lower vertical meridian border between V1 and V2 standing out.

Finally, returning to the lateral surface (see Fig. 2) in the middle of the myelin-dense region of MT+ it is possible to distinguish a border between a posterior orange cluster and an anterior white/tan cluster. A study examining the relation between quantitative T1 and retinotopy [11] surprisingly showed that the heavily myelinated oval in the lateral occipital cortex does not directly correspond to MT; instead, MT proper only accounts for the posterior part of that oval. The anterior part may correspond to FST, which represents parts of the visual field already mapped in MT, and which responds to the ipsilateral visual field unlike MT. Once again, this suggests that diffusion data may help distinguish regions not easily separated by using myelin density alone.

3.5 Gyrification

The unlabeled black arrows on the right of Fig. 4 indicate curvature-like features in the parcellation. These lines follow the fundus and crown of the cingulate sulcus and gyrus respectively. The emergence of these macroscopic landmarks could be associated with sampling errors at areas of high curvature, where partial voluming is more prevalent. Alternatively, it may reflect a relationship between gyrification and diffusion anisotropy, as suggested by several groups—e.g., [21]. Deeper cortical layers appear to thin in sulci, which has been suggested to be a way of maintaining equal local volume by folding-induced tangential stretching [31, 32]. By contrast, upper cortical layers appear to puff out and become more myelinated on gyri. These systematic folding-correlated effects may give rise to detectable differences in grey matter diffusion patterns. The initial detection of a correlation between gyrification and T1 was similarly initially dismissed as a depth-sampling artifact, but then subsequently suggested to be partly due to real myelination differences between sulcal and gyral cortex. An additional complication is that partial volume errors may be detecting systematic differences in fiber direction near the grey/white matter border; for example, the dominant diffusion direction is expected to be highly radial in areas of high curvature, such as gyral crowns, and more tangential in along the banks of gyri due to the angle at which u-fibres project into the cortex [20, 21].

4 Conclusion

We presented a parcellation result using dMRI data, demonstrating areal definitions that reflect some well known architectonically defined regions without the use of a training stage or any non-local spatial constraints. The population average feature set is most discriminative in primary areas that are consistently located across subjects, such as S-I and M-I, and heavily myelinated regions. However, we also observe clusters that may correspond to non-primary areas such as area 44 and 45. Our results demonstrate that the higher-order, diffusion-based, feature set may be distinguishing local differences in the texture and geometry of the myelinated meshwork of the neocortex not all of which are visible in myelin density maps. Incorporating this information is likely to improve the performance of non-supervised multimodal parcellation schemes for cortical areas.

References

1. Brodmann, K.: Vergleichende Lokalisationslehre der Grosshirnrinde in ihren Prinzipien dargestellt auf Grund des Zellenbaues. Barth, Leipzig (1909)
2. Vogt, C., Vogt, O.: Allgemeine ergebnisse unserer hirnforschung, vol. 25. JA Barth (1919)

3. von Economo, C.F., Koskinas, G.N., Triarhou, L.C.: Atlas of Cytoarchitectonics of the Adult Human Cerebral Cortex. Karger, Basel (2008)
4. Zilles, K., Amunts, K.: Centenary of Brodmann's map - conception and fate. Nat. Rev. Neurosci. **11**(2), 139–145 (2010)
5. Amunts, K., Malikovic, A., Mohlberg, H., Schormann, T., Zilles, K.: Brodmann's areas 17 and 18 brought into stereotaxic space – where and how variable? Neuroimage **11**(1), 66–84 (2000)
6. Amunts, K., Schleicher, A., Bürgel, U., Mohlberg, H., Uylings, H., Zilles, K.: Broca's region revisited: cytoarchitecture and intersubject variability. J. Comp. Neurol. **412**(2), 319–341 (1999)
7. Zilles, K., Schleicher, A., Langemann, C., Amunts, K., Morosan, P., Palomero-Gallagher, N., Schormann, T., Mohlberg, H., Bürgel, U., Steinmetz, H., et al.: Quantitative analysis of sulci in the human cerebral cortex: development, regional heterogeneity, gender difference, asymmetry, intersubject variability and cortical architecture. Hum. Brain Mapp. **5**(4), 218–221 (1997)
8. Fischl, B., Salat, D.H., van der Kouwe, A.J.W., Makris, N., Ségonne, F., Quinn, B.T., Dale, A.M.: Sequence-independent segmentation of magnetic resonance images. Neuroimage **23**, S69–S84 (2004)
9. Sigalovsky, I.S., Fischl, B., Melcher, J.R.: Mapping an intrinsic MR property of gray matter in auditory cortex of living humans: a possible marker for primary cortex and hemispheric differences. Neuroimage **32**(4), 1524–1537 (2006)
10. Lutti, A., Dick, F., Sereno, M.I., Weiskopf, N.: Using high-resolution quantitative mapping of R1 as an index of cortical myelination. Neuroimage **93**, 176–188 (2014)
11. Sereno, M.I., Lutti, A., Weiskopf, N., Dick, F.: Mapping the human cortical surface by combining quantitative T1 with retinotopy. Cerebral Cortex **23**(9), 2261–2268 (2013)
12. Glasser, M.F., Van Essen, D.C.: Mapping human cortical areas in vivo based on myelin content as revealed by T1-and T2-weighted MRI. J. Neurosci. **31**(32), 11597–11616 (2011)
13. Glasser, M.F., Goyal, M.S., Preuss, T.M., Raichle, M.E., Van Essen, D.C.: Trends and properties of human cerebral cortex: correlations with cortical myelin content. Neuroimage **93**, 165–175 (2014)
14. Glasser, M.F., Coalson, T., Robinson, E., Hacker, C., Harwell, J., Yacoub, E., Ugurbil, K., Anderson, J., Beckmann, C.F., Jenkinson, M., et al. A multi-modal parcellation of human cerebral cortex. Nature **536**, 171–178 (2016)
15. Leuze, C.W.U., Anwander, A., Bazin, P.-L., Dhital, B., Stüber, C., Reimann, K., Geyer, S., Turner, R.: Layer-specific intracortical connectivity revealed with diffusion MRI. Cerebral Cortex **24**(2), 328–339 (2014)
16. Anwander, A., Pampel, A., Knosche, T.R.: In vivo measurement of cortical anisotropy by diffusion-weighted imaging correlates with cortex type. Proc. Int. Soc. Magn. Reson. Med **18**, 109 (2010)
17. Aggarwal, M., Nauen, D.W., Troncoso, J.C., Mori, S.: Probing region-specific microstructure of human cortical areas using high angular and spatial resolution diffusion MRI. Neuroimage **105**, 198–207 (2015)
18. Deoni, S.C., Jones, D.K.: Time-series analysis of diffusion signal as a model-free approach to segementing tissue. In: *Proceedings of the 14th Annual Meeting of ISMRM*, p. 2734 (2006)
19. Haroon, H.A., Binney, R.J., Parker, G.J.: Probabilistic quantification of regional cortical microstructural complexity. Proc. Intl. Soc. Mag. Reson. Med. **18**, 578 (2010)
20. McNab, J.A., Polimeni, J.R., Wang, R., Augustinack, J.C., Fujimoto, K., Stevens, A., Janssens, T., Farivar, R., Folkerth, R.D., Vanduffel, W., et al.: Surface based analysis of diffusion orientation for identifying architectonic domains in the in vivo human cortex. Neuroimage **69**, 87–100 (2013)
21. Kleinnijenhuis, M., van Mourik, T., Norris, D.G., Ruiter, D.J., van Cappellen van Walsum, A.-M., Barth, M.: Diffusion tensor characteristics of gyrencephaly using high resolution diffusion MRI in vivo at 7T. NeuroImage **109**, 378–387 (2015)
22. Nagy, Z., Alexander, D.C., Thomas, D.L., Weiskopf, N., Sereno, M.I.: Using high angular resolution diffusion imaging data to discriminate cortical regions. PloS ONE **8**(5), e63842 (2013)

23. Wilm, B.J., Nagy, Z., Barmet, C., Johanna Vannesjo, S., Kasper, L., Haeberlin, M., Gross, S., Dietrich, B.E., Brunner, D.O., Schmid, T., et al.: Diffusion MRI with concurrent magnetic field monitoring. Magn. Reson. Med. **74**(4), 925–933 (2015)
24. Sotiropoulos, S.N., Jbabdi, S., Xu, J., Andersson, J.L., Moeller, S., Auerbach, E.J., Glasser, M.F., Hernandez, M., Sapiro, G., Jenkinson, M., et al.: Advances in diffusion MRI acquisition and processing in the human connectome project. Neuroimage **80**, 125–143 (2013)
25. Glasser, M.F., Sotiropoulos, S.N., Anthony Wilson, J., Coalson, T.S., Fischl, B., Andersson, J.L., Xu, J., Jbabdi, S., Webster, M., Polimeni, J.R., et al.: The minimal preprocessing pipelines for the human connectome project. Neuroimage **80**, 105–124 (2013)
26. Uğurbil, K., Xu, J., Auerbach, E.J., Moeller, S., Vu, A.T., Duarte-Carvajalino, J.M., Lenglet, C., Wu, X., Schmitter, S., Van de Moortele, P.F., et al.: Pushing spatial and temporal resolution for functional and diffusion MRI in the human connectome project. Neuroimage **80**, 80–104 (2013)
27. Fischl, B., Sereno, M.I., Tootell, R.B.H., Anders M Dale, et al. High-resolution intersubject averaging and a coordinate system for the cortical surface. Hum. Brain Mapp. **8**(4), 272–284 (1999)
28. Hartigan, J.A., Wong, M.A.: Algorithm as 136: a k-means clustering algorithm. Appl. Stat. **28**(1), 100–108 (1979)
29. White, L.E., Andrews, T.J., Hulette, C., Richards, A., Groelle, M., Paydarfar, J., Purves, D.: Structure of the human sensorimotor system. I: Morphology and cytoarchitecture of the central sulcus. Cerebral Cortex **7**(1), 18–30 (1997)
30. Leonard, C.M., Puranik, C., Kuldau, J.M., Lombardino, L.J.: Normal variation in the frequency and location of human auditory cortex landmarks. heschl's gyrus: where is it? Cerebral Cortex **8**(5), 397–406 (1998)
31. Bok, S.T.: Der einflu\ der in den furchen und windungen auftretenden krümmungen der gro\ hirnrinde auf die rindenarchitektur. Zeitschrift für die gesamte Neurologie und Psychiatrie **121**(1), 682–750 (1929)
32. Waehnert, M.D., Dinse, J., Weiss, M., Streicher, M.N., Waehnert, P., Geyer, S., Turner, R., Bazin, P.-L.: Anatomically motivated modeling of cortical laminae. Neuroimage **93**, 210–220 (2014)